JBIC Journal of Biological Inorganic Chemistry
https://doi.org/10.1007/s00775-022-01980-1

ORIGINAL PAPER

Pb(II) coordination to the nonclassical zinc finger tristetraprolin: retained function with an altered fold

Andrew T. Stoltzfus[1] · Courtney J. Campbell[2] · Madison M. Worth[1] · Kellie Hom[1] · Timothy L. Stemmler[2] · Sarah L. J. Michel[1]

Received: 6 June 2022 / Accepted: 26 October 2022

Abstract

Tristetraprolin (TTP) is a nonclassical CCCH zinc finger (ZF) that plays a crucial role in regulating inflammation. TTP regulates cytokine mRNAs by specific binding of its two conserved ZF domains ($CysX_8CysX_5CysX_3His$) to adenylate-uridylate-rich sequences (AREs) at the 3′-untranslated region, leading to degradation of the RNA. Dysregulation of TTP in animal models has demonstrated several cytokine-related syndromes, including chronic inflammation and autoimmune disorders. Exposure to Pb(II), a prevalent environmental toxin, is known to contribute to similar pathologies, in part by disruption of and/or competition with cysteine-rich metalloproteins. TTP's role during stress as a ubiquitous translational regulator of cell signaling (and dysfunction), which may underpin various phenotypes of Pb(II) toxicity, highlights the importance of understanding the interaction between TTP and Pb(II). The impact of Pb(II) binding on TTP's fold and RNA-binding function was analyzed via UV–Vis spectroscopy, circular dichroism, X-ray absorption spectroscopy, nuclear magnetic resonance spectroscopy, and fluorescence anisotropy. A construct containing the two ZF domains of TTP (TTP-2D) bound to Pb(II) with nanomolar affinity and exhibited a different geometry and fold in comparison to Zn_2-TTP-2D. Despite the altered secondary structure, Pb(II)-substituted TTP-2D bound a canonical ARE sequence more selectively than Zn_2-TTP-2D. Taken together, these data suggest that Pb(II) may interfere with proper TTP regulation and hinder the cell's ability to respond to inflammation.

Graphical abstract

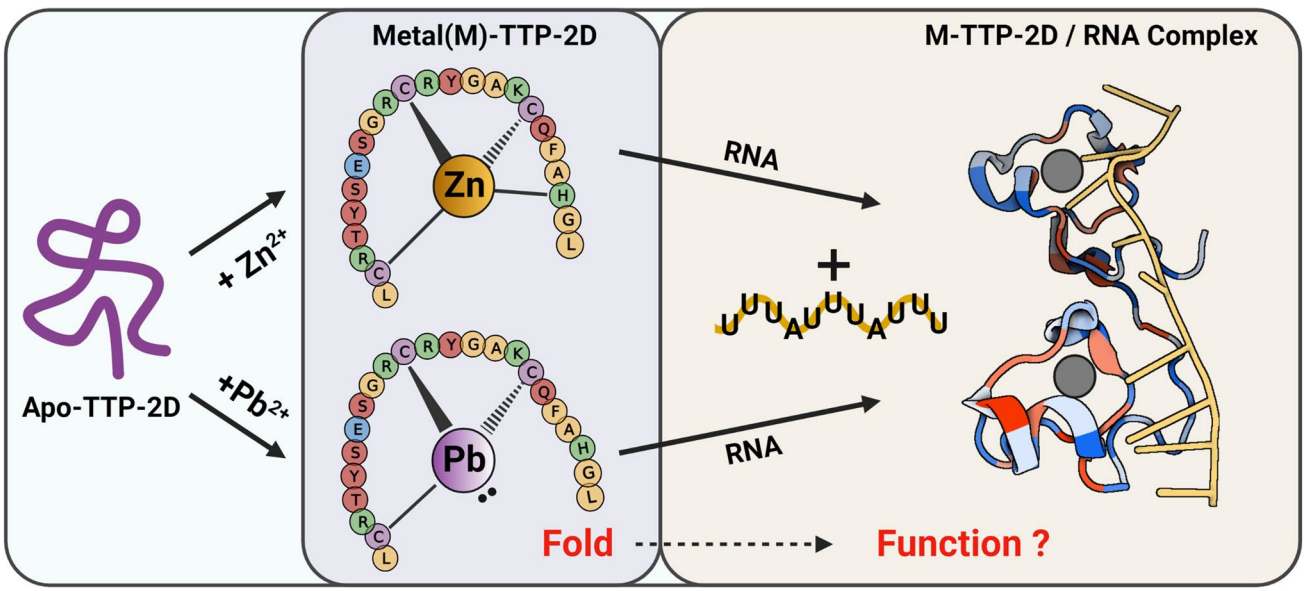

Extended author information available on the last page of the article

Published online: 07 December 2022

Keywords Tristetraprolin · Zinc finger · Pb(II) · Coordination geometry · Protein fold · RNA-binding

Introduction

Pollution of Pb(II) is evident throughout the United States from industrial use and outdated infrastructure, as a result of its low cost and malleability as a metal. Over the last four decades, various federal agencies and departments (EPA, FDA, OSHA, CDC, etc.) have implemented regulations aimed at significantly reducing Pb(II) exposure, which can occur through several environmental routes and consumer products [1–3]. Comparing blood lead levels (BLLs) in children across the U.S. highlights regional differences of Pb(II) exposure, specifically the disproportionate impact on low-income households [4–6]. The National Health and Nutrition Examination Survey (NHANES) has served to monitor the blood lead reference values (BLRVs) for Pb(II), a value that is established based on the 97.5th percentile of Pb(II) burden in children. These BLRVs have decreased since the 1960s, when the BLRV was at 60 µg/dL, to a current value of 3.5 µg/dL. This indicates that the top 2.5% of BLLs in children has reduced dramatically and mean BLL of all children has decreased [7, 8]. However, it is important to note that (1) exposure to Pb(II) can begin early in development through the mother (in utero and with breastfeeding), (2) the BLRV is not based on available scientific evidence, and (3) no safe level of exposure has been determined [9, 10]. Even trace levels of Pb(II) can be associated with significant behavioral and developmental effects. Pb(II) accumulates in the body either in the short-term (blood) or long-term (bone) and is correlated with chronic inflammation, susceptibility to immune disorders, and neurodegeneration [11, 12]. Although the biochemical mechanisms are not fully elucidated, it is understood that Pb(II) interacts promiscuously with metal coordinating motifs in proteins, replacing the native metal, and perturbs a plethora of pathways through oxidative stress and cytokine signaling [12–17].

The cellular targets for Pb(II) toxicity include a wide range of proteins and biomolecules, owing to the intermediate/soft base character of Pb(II), as detailed by the hard–soft–acid–base (HSAB) theory [18]. Its potential to interact with S, O, N, and P ligands underscores the many coordination environments it can adopt and the variety of consequences on the biological system [19]. However, due to Pb(II)'s preference for and tight binding of thiol groups, cysteine-rich biomolecules and proteins have been a focal point for elucidating the mechanism of Pb(II) toxicity. Interaction of Pb(II) with important metalloproteins and competition for their metal binding motifs has been documented in the Ca(II)-binding messenger Calmodulin (CaM), aminolevulinic acid dehydratase (ALAD), metallothioneins (MTs), and zinc fingers (ZFs) [11, 12, 19–31]. Zinc fingers are a broad family of proteins, with 30 different classes currently recognized [32–39]. ZFs all contain motifs of cysteine and histidine with four residues that coordinate Zn(II) in a tetrahedral geometry [32, 38–40]. Zinc is considered a structural cofactor which allows for ZFs to function in transcriptional and/or translational regulation [32, 33, 38, 41]. ZFs are ubiquitous throughout the human body and are essential to maintain proper function of the nervous system, including transcriptional upregulation of MTs, via the ZF metallothionein transcription factor-1 (MTF-1), and MT's ability to sequester xenobiotic metals [26, 42–47]. More broadly, Zn homeostasis (and proper loading/function of ZFs) is crucial in managing inflammatory pathways (i.e., the NF-κB signaling pathway) and cytokine signaling [7, 12, 30, 43, 48].

ZFs have been proposed as biological targets of Pb(II) toxicity, as the ZF sites are thiol rich and thus good ligands for Pb(II) [11, 22]. As such, the CCCH-type and CCCC-types represent the ZF domains that are likely most susceptible to Pb(II) toxicity. The groups of Pecoraro, Penner-Hahn, and Godwin have demonstrated in their use of peptides that correspond to singular ZF domains (~25 to 30 residues) that optimal Pb(II)-binding affinity is achieved with CCCH, CCHC, or CCCC binding domains [21, 23, 24, 27]. Their work established that Pb(II) preferentially binds in a PbS_3 trigonal pyramidal geometry. This finding was further demonstrated with ^{207}Pb-NMR, where Pecoraro and coworkers observed that Pb(II) forms a trigonal complex with three Cys residues, even when four are available [25]. Taken together, along with the work of the Giedroc and Petering groups [49, 50], a hierarchy of Pb(II) binding affinity for Cys-rich/ZF domains of CCCC > CCCH = CCHC > CCHH has been defined [20, 21]. In contrast to this trend, Zawia and coworkers have demonstrated that even Sp-1 and Egr-1, both CCHH-type transcriptional regulators crucial for neurological development, tightly bind Pb(II) and exhibit altered DNA binding [51–53]. In the case of Sp-1, they further elucidated through in vivo rat models that Pb(II) may enhance or inhibit DNA-binding based on the concentration of Pb(II) present. Additionally, Pb(II) inhibited the complex of recombinant Sp-1 and its target DNA, suggesting that Sp-1 is not protected from Pb(II)'s influence by complexation [51]. This demonstrates that although the affinity of Pb(II) for CCHH ZF domains may be orders of magnitude weaker than Zn(II), it can still have detrimental effect. In addition to the CCHH ZFs, GATA ZFs are CCCC-type transcriptional regulators involved in developing the nervous system, as well as the

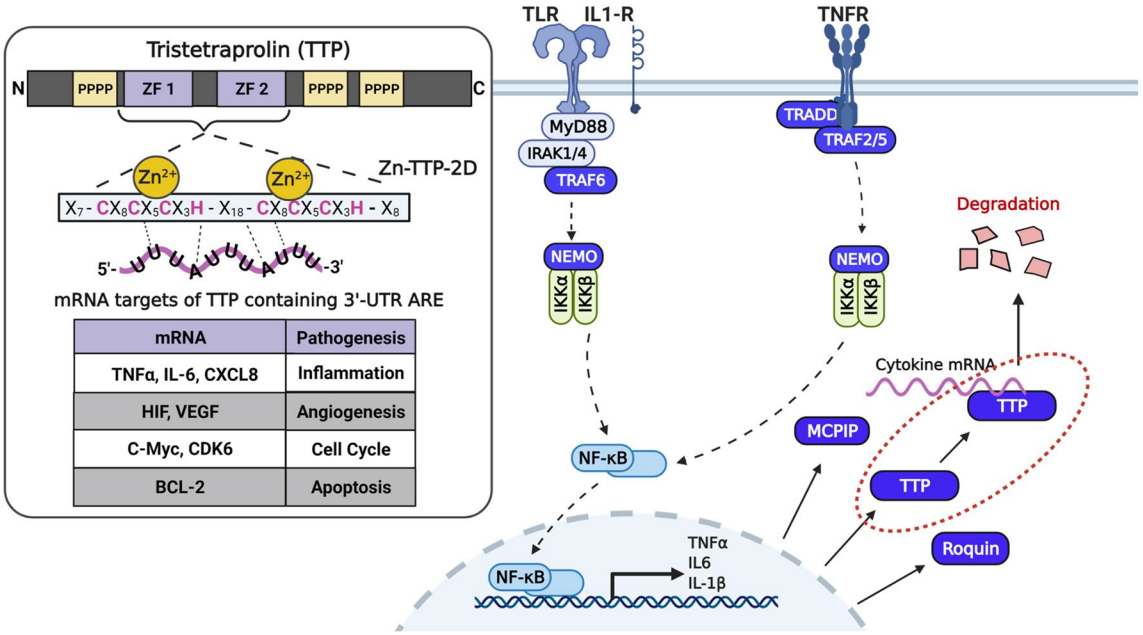

Scheme 1 NF-kB signaling pathway and regulation of cytokine mRNAs by tristetraprolin (TTP). Activation of the pathway through surface receptors (shown here: Toll-Like Receptor [TLR], Tumor Necrosis Factor Receptor [TNFR], and Interleukin-1 Receptor [IL-1R]) leads to translocation of NF-kB to the nucleus and expression of associated cytokine/chemokine genes, increasing mRNA levels of these inflammatory mediators which further activate the pathway. Binding by TTP and other CCCH-type ZFs (MCPIP, Roquin) negatively regulates this signal by decreasing mRNA stability, leading to mRNA degradation, and dampening further signaling of the pathway by mature cytokine/chemokine peptides

cardiovascular and hematopoietic systems [20, 54, 55]. In their work with GATA ZF domains, Godwin and coworkers determined that Pb(II) can replace Zn(II) in the metal site and partially inhibit transcriptional activation [20]. Taken together, these studies support the hypothesis that Pb(II) toxicity, in part, is mediated through displacement of Zn(II) from active sites of critical metalloproteins, including various classes of ZFs.

Tristetraprolin (TTP, NUP475, ZFP36), shown in Scheme 1, is an RNA-binding ZF that negatively regulates the NF-kB pathway by controlling tumor necrosis factor alpha (TNFα) and other cytokines' expression, which further activate the pathway [56–58]. TTP contains two CCCH-type ZF domains that each bind a Zn^{2+} cofactor and adopt a structure with limited alpha-helical character and some loops around the metal site [59]. This folding event allows for tight and specific binding of adenylate-uridylate rich elements (AREs) in the 3'-UTR of cytokine mRNA, with each ZF domain binding a minimum sequence of 5'-UAUU-3' [59]. The binding of TTP to AREs allows for recruitment of the CCR4-NOT1 protein complex and/or the DCP1/DCP2 decapping complex, destabilizing the mRNAs, ultimately reducing their overall translation and ability to further potentiate signaling [60]. Approximately 26% of human mRNA 3'-UTRs contain at least one TTP binding site of 5'-UA$(U)_{3\text{-}5}$AU-3' and proper TTP function has been demonstrated as a vital factor in several disorders, including inflammation, apoptosis, cancer, and immune-related diseases [61–68]. TTP's role in managing cytokine expression and limiting inflammation connects it to the deleterious effects of Pb(II) toxicity, in addition to the potential for Pb/Zn competition for the metal site. Recent work from our laboratory and others demonstrated that e-cigarettes and other aerosolizing devices may contribute to heavy metal exposure, namely Pb(II) [69]. As e-cigarettes are becoming a popular and so-called "safe" alternative to cigarettes, their use is on the rise, specifically in high school students where it is the major form of tobacco use [70, 71]. This trend represents another possible route of exposure to Pb(II) by the general public and particularly in the developing bodies of adolescents and young adults. We hypothesize that Pb(II) targets TTP during exposure, disrupting the native conformation, ultimately affecting the function of TTP.

To determine how Pb(II) affects TTP structure and function, we performed a series of experiments on the CCCH-type ZF, TTP, which has a pivotal role in regulating the pathologies associated with Pb(II) toxicity. Interactions between Pb(II) and the two-domain construct, TTP-2D, were assessed via several spectroscopies to examine how Pb(II) would affect the structure and function of the RNA-binding ZF domains of TTP. We show that Pb_2-TTP-2D exhibits a dissimilar fold to Zn_2-TTP-2D while retaining tight and

specific binding for a canonical mRNA ARE sequence. Notably, the relative affinities for altered RNA sequences were significantly weaker for Pb_2-TTP-2D than Zn_2-TTP-2D, suggesting that Pb_2-TTP-2D may be more selective for target RNA than the native Zn_2-TTP-2D. As such, we propose that Pb(II) may serve as a functional mimic of Zn(II) for TTP binding activity, either over activating mRNA decay or stalling it by preventing necessary protein–protein interactions (PPIs).

Materials and methods

Pb(II) acetate trihydrate ($Pb(OAc)_2$), acetonitrile, trifluoroacetic acid (TFA), and Chelex 100 sodium resin were purchased from Sigma. Pb(II) nitrate atomic absorption standard ($PbNO_3$ AAS; 4.3 mM in 2% nitric acid) was purchased from Fluka Analytical. Zinc(II) chloride ($ZnCl_2$), cobalt(II) chloride ($CoCl_2$), dithiothreitol (DTT), deuterium oxide (D_2O), and HEPES (free acid and sodium salt) were purchased from Sigma-Aldrich. 2-(*N*-morpholino) ethanesulfonic acid sodium salt (MES) was purchased from VWR. Tris(hydroxymethyl)aminomethane (Tris)-HCl was purchased from Promega. Tris base was purchased from Fisher. 3 kD molecular weight cutoff (MWCO) centrifugal spin-filters (0.2 µM polyethersulfur (PES) membrane) were purchased from Millipore Sigma. All buffers were prepared with Chelex-treated Milli-Q water, filtered through a 0.2 µM PES membrane (VWR), degassed via vacuum purging/N_2-sparging, and stored in a Coy anaerobic chamber (3% H_2/97% N_2). $Pb(OAc)_2$, $ZnCl_2$, and $CoCl_2$ metal salts were prepared in degassed Chelex-treated Milli-Q water. $PbNO_3$ AAS was diluted to working stocks with 100 mM HEPES buffer, pH 7.5. All metal solutions were then syringe-filtered and stored in the Coy anaerobic chamber.

TTP-2D sample preparations and anaerobic measurements

Unless otherwise specified, all TTP-2D manipulations and UV–visible titrations were performed in a Coy anaerobic chamber (3% H_2/97% N_2). UV–visible spectroscopy was performed in 1 cm pathlength quartz cuvettes (Starna Cells) using a Cary 60 UV–Vis Spectrophotometer (Agilent). For circular dichroism (CD) and fluorescence anisotropy (FA), samples were prepared in the anaerobic chamber with 1 mm quartz and 5 mm Spectrosil quartz cuvettes (Starna Cells), respectively, and Teflon-stoppered for measurements outside the Coy anaerobic chamber. All analyses were performed in triplicate.

TTP-2D overexpression and purification

A two-domain construct of TTP (TTP-2D), containing both CCCH zinc finger domains was prepared as previously reported [72, 73]. The expression vector, a pET-15b vector ligated with the gene for AA 94–166 of *Zfp36,* encoded the following sequence: SRYKTELCRTYSESGRCRYGAKCQFAHGLGELRQANRHPKYKTELCHKFYLQGRCPYGSRCHFIHNPTEDLAL. The vector was transformed into BL21 (DE3) competent cells and the cells were incubated in Luria–Bertani (LB) medium containing 100 µg/mL ampicillin at 37 °C until mid-log phase, around an OD_{600} of 0.6–0.8. A solution of 1 mM isopropyl β-D-1-thiogalactopyranoside (IPTG) was then added to the incubation flasks to promote protein expression. At 4 h post-induction, cells were centrifuged at 7000 rpm for 20 min at 4 °C. The cell pellet was resuspended in a lysis buffer consisting of 8 M urea, 10 mM MES buffer, pH 6 with an EDTA-free protease inhibitor mini-tablet. Dithiothreitol (DTT) was added to the resuspension for a final concentration of 10 mM to prevent oxidation of the cysteinyl sulfur groups during purification. Cell lysis was performed on ice via sonication (Fisher Scientific Sonic Dismembrator Model 100). Centrifugation of the cell lysate at 5000×*g* for 20 min at 4 °C yielded a distinct pellet and supernatant. The pellet was discarded while the supernatant was applied to an SP-sepharose column and incubated at room temperature while rocking for 1 h. A separation gradient of sodium chloride was prepared in similar lysis buffer (4 M urea) and was applied to the column from 0 to 2 M NaCl, with TTP-2D eluting at 600 mM NaCl. An additional 25 mM DTT was applied to the elution and incubated at 56 °C for 2 h to ensure full reduction of thiol bonds. TTP-2D was subsequently purified via either a Waters HPLC or Agilent HPLC with a C-18 column using reverse phase chromatography. A gradient of H_20/CH_3CN, both containing 0.1% TFA, was applied to elute TTP-2D at 32% CH_3CN. Elutions were immediately placed in a Coy anaerobic chamber (97% nitrogen/3% hydrogen) and lyophilized to dryness. Peptide was confirmed for purity and metal-binding ability by SDS-PAGE and UV–visible spectroscopy. Further protein manipulations and sample preparations were made in the anaerobic chamber.

Direct titration of apo-TTP-2D with Pb(II) and Zn(II)

The optical spectrum of TTP-2D was measured from 220 to 820 nm as Pb(II) was added to the protein. A solution of apo-TTP-2D (typically 17 µM) in 100 mM HEPES buffer, pH 7.5 was titrated with $Pb(OAc)_2$ up to 2 molar equivalents (in increments of 0.2), followed by larger additions until 20 total equivalents Pb(II) were added. The Pb_2-TTP-2D solution was then titrated in the same manner with $ZnCl_2$. The

changes in the absorption band at 336 nm with Pb(II) and Zn(II) addition were monitored.

Job plot by UV–visible spectroscopy

Apo-TTP-2D and $Pb(NO_3)_2$ were kept at a constant total concentration of 20 μM in 100 mM HEPES, pH 7.5 and analyzed by UV–Visible spectroscopy from 220 to 820 nm. Peptide/Pb(II) solutions were prepared where the mol fraction of Pb(II) in each reaction was varied as 0.10, 0.31, 0.36, 0.41, 0.51, 0.69, 0.72, 0.92. Corrected absorbance ($A - A_0$) at 260 and 336 nm were used to generate the Job Plot; mole fraction (X_a) of Pb(II) vs the corrected absorbance, where mole fraction = [Pb(II))]/{[Pb(II) + [apo-TTP-2D]} [74–76].

Competition titrations of Co(II)-TTP-2D with Pb(II) or Zn(II)

Co_2-TTP-2D was prepared and analyzed by UV–visible spectroscopy from 220 to 820 nm. A solution of apo-TTP-2D (42 μM) in 100 mM HEPES, pH 7.5 buffer was titrated with an excess of $CoCl_2$ (2.4 molar equivalents) and the characteristic d-d transition bands between 600 and 700 nm of tetrahedral Co(II) binding were monitored. Then Pb(II) or Zn(II) were added (increments of 0.4, 0.8, 1.2, 1.6, 2.0, 2.4, and 2.8 molar equivalents) to observe the disappearance of the d-d transition bands, indicative of either Pb(II) or Zn(II) displacement of Co(II) from the TTP-2D metal-binding domains. In separate experiments, apo-TTP-2D (~ 20 μM) was titrated with 15 equivalents of $CoCl_2$ and the absorbance at 650 nm (the maximum of the Co(II) d-d absorption bands) was fit to a 1:1 binding equilibrium with linear, least squares analysis (KaleidaGraph, Synergy Software). The relative affinity of TTP-2D for Pb(II) was then determined by adding $Pb(OAc)_2$ in equal fashion to the forward titration and monitoring the loss of d-d band absorbance at 650 nm. An upper limit dissociation constant (K_d) for Pb(II) was determined by fitting the data to a competitive binding equilibrium (below) previously reported by our laboratory and others [72, 77].

$$Co_2\text{-TTP-2D} + Pb(II) \underset{K_d^{Pb}}{\Leftrightarrow} Pb_2\text{-TTP-2D} + Co(II)$$

Circular dichroism (CD) spectroscopy

Circular dichroism (CD) spectra for M-TTP-2D ($M = Pb^{2+}$ or Zn^{2+}) were measured between 200 and 250 nm using a Jasco-1500 spectropolarimeter set for high sensitivity. Scanning speed was 50 nm/min, with 4 nm bandwidth, and 4 s response time. A total of four scans were collected and displayed as an average for the final plot. A peptide concentration of 30 μM ([M] = 60 μM) was prepared in 10 mM tris buffer, pH 7.5. Apo peptide was first scanned followed by a scan with 2-eq of either Pb(II) or Zn(II), with both corrected for the initial spectrum obtained of buffer alone.

X-Ray absorption spectroscopy (XAS)

A Pb_2-TTP-2D sample was prepared for XAS by mixing apo-TTP-2D with a slight excess of $Pb(OAc)_2$ in 200 mM HEPES buffer, pH 7.5. The sample was then concentrated and desalted with a 3 kD MWCO spin filter. Finally, dilution with 200 mM HEPES buffer containing 60% glycerol yielded a Pb_2-TTP-2D sample at 1 mM peptide, 2 mM Pb(II), and 30% glycerol (%v/v).

X-ray absorption spectra at the Pb(II) L_3-edge were collected at the Stanford Synchrotron Radiation Lightsource (SSRL) on beamline 7–3. Beamline 7–3 utilized a Si[220] double crystal monochromator with an inline mirror for X-ray focusing and for harmonic rejection. During data collection, Pb-loaded TTP2D samples were maintained at 10°K using a liquid He continuous flow cryostat. Fluorescence XAS spectra were collected using a 30 element Ge detector from Canberra. Spectra were collected in 5 eV increments in the pre-edge region (12,830–13,040 eV), 0.25 eV increments in the edge region (13,040–13,080 eV) and 0.05 $Å^{-1}$ increments in the extended X-ray absorption fine structure (EXAFS) region (out to $k = 13$ $Å^{-1}$), integrating from 1 to 25 s in a k^3 weighted manner for a total scan length of approximately 50 min. The X-ray energy in each spectrum was calibrated individually by collecting a Pb-foil absorption spectra simultaneously with the compound spectra, utilizing the Pb(II) foil L_3-edge at 13,055 eV.

XAS spectra were processed using the Macintosh OS X version of the EXAFSPAK program suite [78] integrated with the Feff v8 software [79] for theoretical model generation. Data reduction utilized a Gaussian spline for background removal in the pre-edge region and a three-region cubic spline throughout the EXAFS. Data were converted to k-space using a Pb(II) E_0 value of 13,080 eV. The k^3 weighted EXAFS was truncated at 12.0 $Å^{-1}$ due to the intense presence of monochromator crystal imperfections in the data above this value. This k range corresponds to a spectral resolution of ca. 0.14 Å for all lead-ligand interactions; therefore, only independent scattering environments outside 0.14 Å were considered resolvable in the EXAFS fitting analysis [80]. EXAFS fitting analysis was performed first on filtered data and then verified on the raw unfiltered data. EXAFS data were fit using single scattering amplitude and phase functions calculated with the program Feff v8. Single scattering theoretical models were calculated for carbon, nitrogen, and sulfur coordination to simulate lead nearest-neighbor ligand environments. Scale factor (Sc) and E_0 values, used in a static manner during the simulations, were calibrated by fitting crystallographically characterized

Pb(II) solid state models; specific values include a Scale Factor of 0.7 and E_0 values of − 20 eV for N/C and − 24 eV for S interactions. Criteria for judging the best-fit simulation utilized both the lowest mean square deviation between data and fit (F'), corrected for the number of degrees of freedom, and a reasonable Debye–Waller factor [81, 82].

Fluorescence anisotropy (RNA binding)

A K2 spectrofluorometer (ISS, Inc.) was configured in the L format for all fluorescence anisotropy (FA) experiments. Excitation and emission wavelengths were set at 495 and 517 nm, respectively, each with a band pass of 2 nm. Cuvettes were prepared with 10 nM RNA in a 200 mM HEPES/100 mM NaCl buffer containing 0.1 mg/mL bovine serum albumin (to prevent non-specific binding) at pH 7.5. The anisotropy (r) of unbound RNA was measured as a function of M-TTP-2D added to the cuvette. Each data point is an average of 22 readings over 60 s. Raw anisotropy values were converted to fraction bound (F_{bound}; the fraction of RNA bound to Pb_2-TTP-2D at a given RNA concentration), via the following equation:

$$F_{\text{Bound}} = \frac{r - r_{\text{Free}}}{(r_{\text{Bound}} - r)Q + (r - r_{\text{Free}})}$$

where r_{free} is the anisotropy of the unbound RNA in the initial scan, r_{bound} is the anisotropy of the RNA–protein complex at the point of saturation, and Q is the quantum yield ($Q = \text{Intensity}_{bound}/\text{Intensity}_{free}$). Q is applied as a correction factor to account for change in fluorescence intensity throughout the titration. A plot of F_{Bound} as a function of M-TTP-2D addition to the RNA was fit using KaleidaGraph (Synergy Software) with a 1:1 binding model, considering the following equilibria and equation, where P is the [M-TTP-2D] and R is the [RNA]:

$$P + R \overset{Kd}{\Longleftrightarrow} PR$$

$$K_{\text{D}} = \frac{[P][R]}{[PR]}$$

$$F_{\text{Bound}} = \frac{\left(\left(P_{\text{Total}} + R_{\text{Total}} + K_{\text{D}} - \sqrt{P_{\text{Total}} + R_{\text{Total}} + K_{\text{D}} - 4P_{\text{Total}} \times R_{\text{Total}}}\right)\right)}{2R_{\text{Total}}}$$

NMR spectroscopy

NMR experiments were performed with an Agilent DD2 500 MHz spectrometer at 25.0 °C. Both 1-D and 2-D experiments used approximately 350 µM apo-TTP-2D prepared in D_2O or H_2O and pH-adjusted to 6.5 with a solution of tris(hydroxymethyl)aminomethane (tris) in D_2O. Metal stocks used were prepared in D_2O. After metal addition, pH was verified and adjusted to 6.5 (if necessary) with tris in D_2O.

1-D NMR experiments were performed in 100% D_2O with instrument parameters of 32 transients, 16,384 total points, 5 s relaxation time, and a spectral width of 6009 Hz. 2-D gCOSY experiments were performed in (90%/10%) H_2O/D_2O with a spectral width of 8102 Hz, 2 s of delay between transients immediately followed by 1 s of presaturation to suppress the solvent signal, 32 transients, 4096 total points per fid, and 400 indirectly detected increments. Transmitter offset was set on the residual water peak for all experiments.

Results and discussion

TTP-2D as a model for Pb(II) binding of CCCH type zinc fingers

TTP is a 'CCCH' type ZF protein that contains two conserved Cys_3His ZF domains. TTP regulates cytokine and chemokine mRNAs that are related to several inflammatory and chronic pathologies, including cancer, arthritis, and autoimmunity [62, 63, 83]. TTP achieves this regulation by binding to AU-rich elements present at the 3′-UTR of cytokines and chemokines. Upon TTP/RNA binding, the CCR4-NOT1 protein complex and/or the DCP1/DCP2 decapping complex associate with TTP/RNA leading to destabilization of the mRNAs [58, 60]. RNA binding by TTP requires only the two CCCH domains. We have previously reported that a construct of TTP (TTP-2D) containing the tandem-ZF domains can bind zinc, adopt secondary structure, and function (i.e., bind to a canonical ARE sequence), making it an appropriate construct to examine the effect of Pb(II) binding [73, 84, 85]. Moreover, the approach of utilizing single- and multi-ZF domain peptides to interrogate metal binding, structure, and function for ZFs is commonly used in their study [33, 49, 86, 87]. Here, we over-expressed and purified TTP-2D, and isolated in the apo-form for metal binding and functional studies [72].

Characterization of Pb(II) binding to TTP-2D

Apo-TTP-2D was titrated with $Pb(OAc)_2$ to determine whether Pb(II) binds to TTP-2D. Upon addition of $Pb(OAc)_2$

an intense absorption band centered at 235 nm with a shoulder at 260 nm was observed. In addition, a well-resolved but less intense absorption band was seen at 336 nm (Fig. 1a). These bands suggest that Pb(II) is binding to apo-TTP-2D. We propose that these bands are ligand-to-metal charge transfer (LMCT) and intra-atomic transitions with Pb(II) based upon early Pb–S site studies by the Godwin and Pecoraro groups [23, 27]. Extinction coefficients for the absorbance at 260 nm ($\mathcal{E}$ = ca. 12,000 M^{-1} cm^{-1} per domain) and 336 nm ($\mathcal{E}$ = ca. 3,600 M^{-1} cm^{-1} per domain) were determined. These values are in agreement with those reported as charge transfer bands between sulfur and Pb(II) by Giedroc, Pecoraro, and Jalilehvand, and offer further support for Pb–S binding [24, 25, 88, 89]. Increases in the absorbance bands at 260 and 336 nm were observed until 2 molar equivalents of $Pb(OAc)_2$ had been titrated (Fig. 1b), indicative of a 2:1 stoichiometry of binding (2Pb: 1TTP-2D). This stoichiometry was further supported by applying the method of continuous variation with respect to the absorbance at 260 and 336 nm. The Job Plot in Fig. 1c shows that the optimal absorbance value for the Pb–S LMCT at 336 nm is at a mole fraction for Pb(II) of 0.66, further supporting the 2:1 binding stoichiometry.

To confirm that Pb(II) indeed binds TTP-2D in the CCCH ZF domains and to determine a dissociation constant (K_d), apo-TTP-2D was first bound with excess Co(II) (15 equivalents) and then titrated with Pb(II). Co(II) is a common spectroscopic probe for Zn(II) binding to ZF domains, as Zn(II) is a spectroscopically silent metal due to its d^{10} shell and affinities cannot be directly determined [34, 72, 73, 77, 85, 90–93]. Co(II) has a d^7 electron shell and exhibits distinct d-d transition bands between 550 and 750 nm when coordinating ligands in a tetrahedral geometry. In the case of TTP-2D's CCCH domains, Co(II) d-d transition bands are observed from 600 to 700 nm, with maxima at ca. 650 and 675 nm, and a shoulder at ca. 600 nm. The same competitive binding approach was performed for Pb(II). As shown in Fig. 2a, we observed a loss of the d-d bands upon titration with Pb(II), indicative of Pb(II) binding to TTP-2D at the same site as Co(II) (and by inference Zn(II)). The data were fit to a competitive binding equilibrium and yielded a dissociation constant (K_d) of 9.0×10^{-9} M (Fig. 2b), which compares closely to that of Cd(II) for TTP-2D ($K_d = 3.5 \times 10^{-9}$ M) and is in-line with the reported Pb(II) affinities for Cys_3 sites (Table 1) [84] (Fig. 2).

Binding affinities of other lead finger peptides are presented in Table 1 as dissociation constants (K_d). The preference for thiolate sites is demonstrated by the consensus peptides and typical site preference of CCCC > CCCH = CCHC > CCHH. Although Pb(II) does not bind TTP-2D as tightly as Zn(II), it binds more tightly than Co(II) and Fe(III) (3.5×10^{-6} M and 3.0×10^{-5} M, respectively) [1], and in the same order of magnitude (10^{-9} M) as Cd(II), which has been shown to displace Zn(II) from TTP-2D in native ESI–MS experiments [94]. We note that Godwin and others have reported nano- and even picomolar Pb(II)-binding of ZF peptides often using consensus peptide (CP) sequences which are optimized and often lead to tighter metal binding affinities than peptides based on wild-type proteins [20, 21]. In addition to the binding affinity of Pb(II) for TTP-2D, the absorption bands and maxima compare well to the available literature.

Structure and coordination geometry of Pb_2-TTP-2D

Circular dichroism

To understand the impact of Pb(II) binding on secondary structure, circular dichroism (CD) was employed. While classical zinc finger domains (CCHH-type) adopt a well-defined ββα fold upon Zn(II) addition [91, 95], the nonclassical CCCH ZF domains of TTP gain a small but measurable change in structure with Zn(II) [38]. Figure 3a shows the CD spectra of apo-TTP-2D and Zn_2-TTP-2D and reveals that Zn(II) addition induces some secondary structure compared to the apo-peptide, indicated by the small peaks centered at 218 and 227 nm. These data are supported by the findings of Wright and coworkers on Tis11D, a close homolog of TTP and a member of the same ZFP36 family, that revealed that Zn(II) imparts limited structure to the apo-ZF [59]. In comparison to the native Zn(II) cofactor, Pb(II) addition leads to a different CD spectrum (Fig. 3a) which more closely resembles the apo-TTP-2D spectrum. Additionally, in Fig. 3b, a Zn_2-TTP-2D sample titrated with molar equivalents of $Pb(OAc)_2$ exhibited immediate and stepwise shifts in the CD spectra from 215 to 230 nm, the region attributed to alpha-helical structure gained from Zn(II) coordination. The final CD spectrum resembles the spectrum observed for Pb_2-TTP-2D (Fig. 3a), suggesting that Pb(II) is affecting the secondary structure of folded Zn_2-TTP-2D.

The finding that Pb(II) binding to TTP-2D does not induce changes in secondary structure as measured by CD is consistent with the data we have reported for TTP-2D binding to other non-native metals Cd(II) and Cu(I) [84, 85]. While the spectrum for Cu_2-TTP-2D resembles the Pb_2-TTP-2D spectrum presented in Fig. 3a, the CD spectrum for Cd_2-TTP-2D does have peak character/spectral shape closer to that of Zn_2-TTP-2D, although the CD signal intensities and overall shapes are not superimposable. This may relate to chemical similarity between Cd(II) and the native Zn(II) cofactor, as they are both d^{10} metals that adopt similar geometries [19, 84]. In addition, Pb(II) does not induce a stable secondary structure in other types of ZFs. For example, Godwin and coworkers found that Pb binding to ZF constructs of either the HIV nucleocapsid domain (CCHC) or ZF CP-1 (CCHH) show limited secondary structure

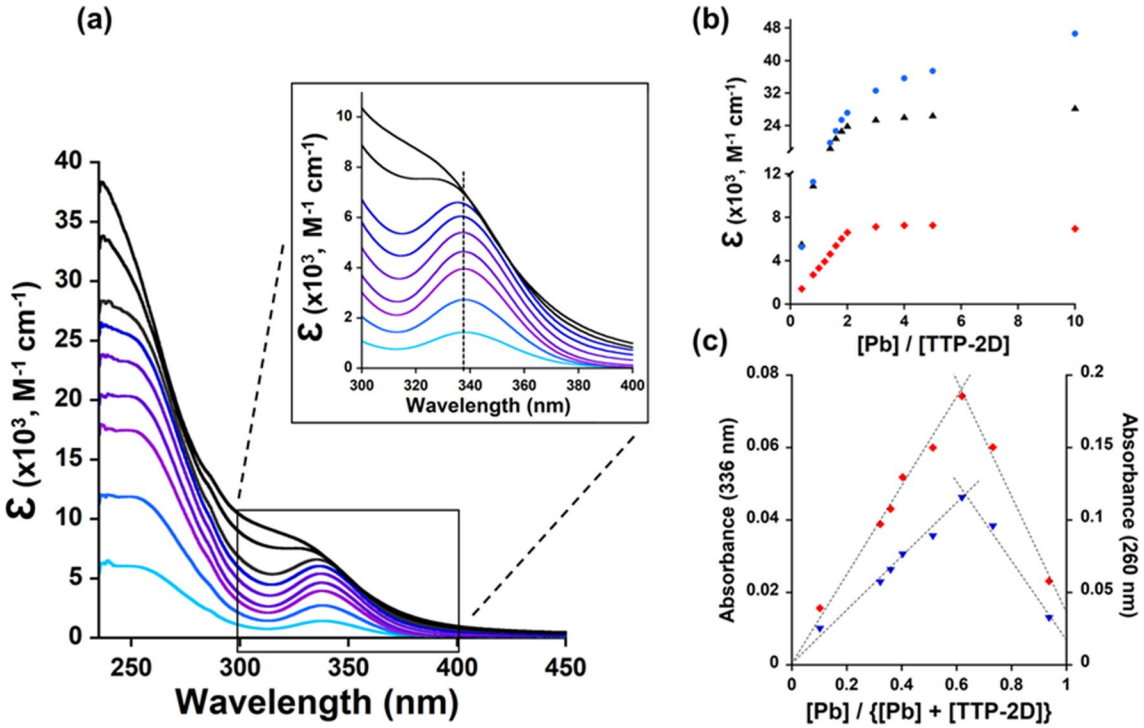

Fig. 1 **a** Plot of the change in the absorption spectrum between 230 and 450 nm as apo-TTP-2D (20 μM) is titrated with 0.4, 0.8, 1.2, 1.4, 1.6, 1.8, 2, 3, and 5 equivalents of $Pb(OAc)_2$ (inset: magnified plot of the change in the same absorption spectrum between 300 and 400 nm at the same equivalents of $Pb(OAc)_2$). **b** Plot of the increase in absorbance at 235 nm (blue circle), 260 nm (black triangles), and 336 nm (red diamonds) as apo-TTP-2D is titrated with $Pb(OAc)_2$. **c** Job plot of Pb^{2+}/apo-TTP-2D interaction where absorbance at both 260 (red diamonds) and 336 nm (blue triangles) are plotted against the mole fraction of Pb^{2+}, where mole fraction = $[Pb^{2+}]/\{[Pb^{2+}]+[\text{apo-TTP-2D}]\}$. Total concentration of $[Pb^{2+}]+[\text{apo-TTP-2D}]$ was maintained at 20 μM for each data point. All above experiments were performed in 100 mM HEPES buffer, pH 7.5

Table 1 Dissociation constants (K_d), in (M), of reported ZF peptides

Zinc finger peptide	K_d Zn(II)	K_d Pb(II)	References
TTP-2D	6.2×10^{-11}	9.0×10^{-9}	Zn:[1], Pb: this work
HIV-CCHC	7.0×10^{-11}	3.0×10^{-10}	[20]
CP-CCHH	5.7×10^{-12}	5×10^{-11}	[20]
CP-CCHC	3.2×10^{-12}	8×10^{-11}	[20]
CP-CCCC	1.1×10^{-12}	3.9×10^{-14}	[20]
Ros87	5.8×10^{-10}	5.6×10^{-6}	[18]
TFIIIA (F3)	1.0×10^{-8}	3.4×10^{-8}	[17]

when measured by CD [21]. Similarly, a study using a Cys-containing peptide model by Pecoraro and coworkers demonstrated that alpha-helical character could be induced by Zn(II) addition but not by Pb(II) [24]. Finally, Isernia and coworkers showed that several metals, including Pb(II), did not induce conformational changes in the classical ZF Ros87 [86].

2-Dimensional ^{1}H-nuclear magnetic resonance (NMR) spectroscopy

Due to the predominantly tetrahedral coordination of Zn(II) across all classes of ZFs, in contrast to the propensity for trigonal pyramidal binding of Pb(II) in biomolecules, the differences in chemical environments of TTP-2D's amino acid side chains would presumably be significantly different when bound to either metal [23]. To probe the proton environment upon Pb(II) binding, 2-D COSY ^{1}H-NMR was utilized to compare Pb- and Zn-bound TTP-2D. In Fig. 4, overall chemical shift dispersion demonstrates a lack of well-defined proton cross-peaks in the Pb_2-TTP-2D sample. The crosspeaks between the backbone amide (6–9.5 ppm) and the alpha-protons of the residues (3–4.5 ppm) in the Zn-bound spectrum are well-dispersed and those in the Pb-bound spectrum are not. The intra-residue crosspeaks of the aromatic sidechain residues (Tyr, Phe, His) are also different between the Zn- and Pb-bound forms, as there are more of these crosspeaks in the Zn-form, and they are more dispersed as well. Our chemical shift dispersion results agree with the findings of Godwin and coworkers, who reported that Pb(II) binding of an HIV-CCHC construct does not fully fold the

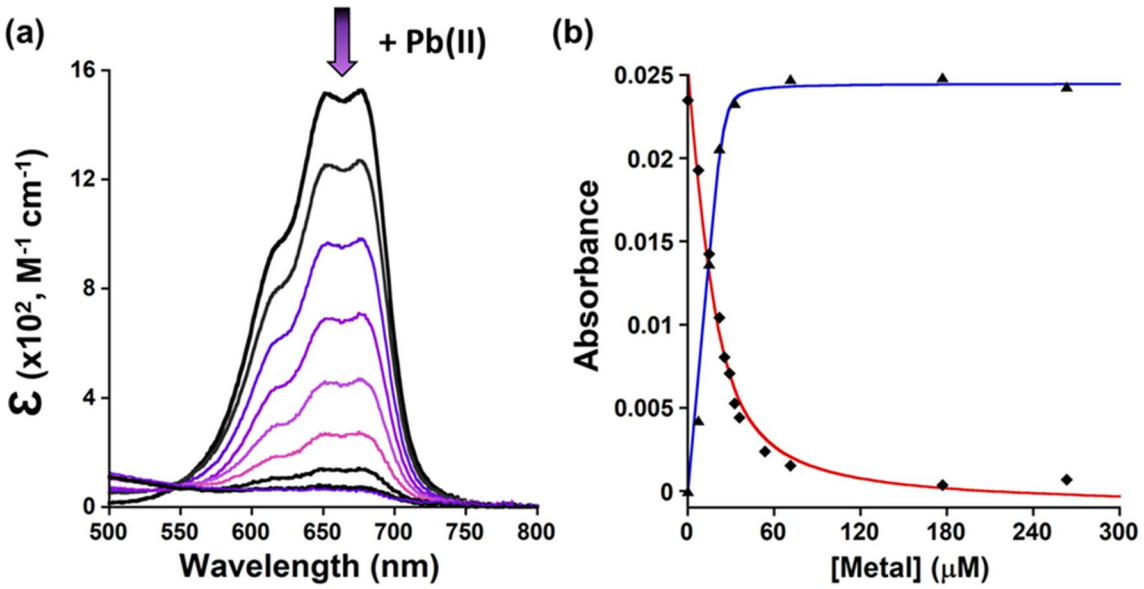

Fig. 2 **a** Plot of the change in the absorption spectrum between 500 and 800 nm, as 0.4, 0.8, 1.2, 1.6, 2.0, 2.4, and 2.8 equivalents of $Pb(NO_3)_2$ is added to Co_2-TTP-2D. **b** Plot of the change in the absorption spectrum at 650 nm as a function of concentration as Co^{2+} (blue) is added to apo-TTP-2D and Pb^{2+} (red) is added to Co_2-TTP-2D. Both titrations were performed with ~ 20 μM apo-TTP-2D in 100 mM HEPES buffer, pH 7.5

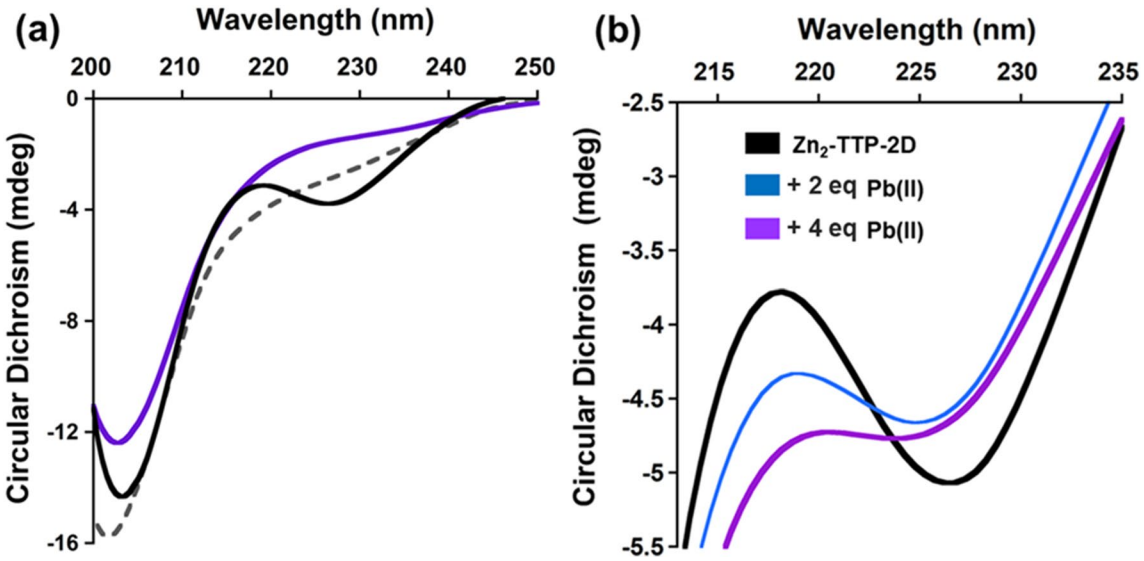

Fig. 3 **a** Overlay of the CD spectra of apo-TTP-2D (black dashed line), Zn-TTP-2D (black line), and Pb-TTP-2D (purple). **b** Overlay of the CD spectra for Zn-TTP-2D (black line) and following additions of $Pb(OAc)_2$ (2-eq: blue line, 4-eq: purple line). All experiments were performed starting with 30 μM apo-TTP-2D in 10 mM tris buffer, pH 7.5

peptide or influence the proton environment in the way that Zn^{2+} does [21]. Furthermore, these NMR data are supportive of the CD data (Fig. 3a, b) that Pb(II) has a notably different impact on peptide fold/structure in comparison to Zn(II).

Extended X-ray absorption fine structure (EXAFS)

X-ray absorption spectroscopy (XAS) was utilized to elucidate the geometry of Pb(II) binding, as well as its coordinating ligands and near/long range interactions. XAS data collected on the Pb(II) L_3-edge for Pb_2-TTP-2D provided a structural picture of metal coordinated in a PbS_3 ligand

environment (Fig. 5). Simulations of the EXAFS data showed the nearest neighbor environment of Pb(II) was dominated by sulfur scattering at 2.66 Å (Fit 1, Table 2). The simulation parameter with the highest accuracy within this technique is the bond length (at ± 0.02 Å), and the Pb–S value of 2.66 Å agrees closely with reported Pb-S_3 bond lengths in both proteins and small molecules bound to Pb(II) [23, 96, 97]. Although the Pb–S bond length is most consistent with a trigonal pyramidal Pb–S_3 complex [23], the best fit coordination number (CN) we obtained from the simulation was lower at 2.0; the accuracy of this parameter in the simulation is ± 1.0 [81]. We believe the apparent simulation number of 2.0 is lower than the actual value of 3.0 due to the high disorder between the 3 individual bonds, as indicated by the high Debye–Waller bond disorder factor. During the simulations, the Debye–Waller factors were $> 5 \times 10^3$, indicating that there is substantial disorder between the individual Pb–S direct bonds, although the average bond length was at 2.66 Å. A similar disconnect in EXAFS simulations between clear three coordinate Pb sample architecture, based on the high accuracy of bond length values obtained in the fits, and an unrealistically low 2 coordinate coordination number from the fit was also observed by Godwin and Penner-Hahn [23]. In their CCHC peptides, their data predict a CN of 2 sulfur scatterers which yielded a lower Debye–Waller factor than a fit with a CN of 3, and this was a result of destructive overlap of the EXAFS signals from the mixed Pb–S and Pb–N/O scatterers. We conjecture that a Pb-S_3 coordination environment is therefore most consistent with our simulation results. Contributions from long range carbon scattering at 3.04 Å (Fit 2, Table 2) and finally at 4.18 Å provide the optimal simulation metrical parameters for Pb(II) bound to TTP-2D (Fit 3, Table 2).

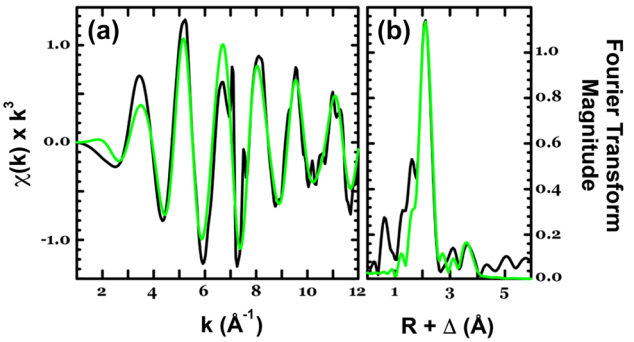

Fig. 5 Pb L3 Edge EXAFS (**a**) and Fourier transform of the EXAFS (**b**) for Pb_2-TTP-2D. Raw/unfiltered data shown in black while simulated data is shown in green

Our XAS data are consistent with additional characterized three coordinate Pb(II) coordination sites found in both proteins and biomolecules [22, 89]. The Penner-Hahn and Giedroc groups highlighted the preference for PbS_3 coordination in the metalloregulator CadC [88]. Similarly, in 2005 work that was focused on the consensus ZF peptide CP and related mutations, the Godwin and Penner-Hahn groups reported a preference of Pb(II) for trigonal pyramidal sites for Pb binding to a series of modified CP peptides (CP-CCHC, CP-CCCH, and CP-CCCC) [23]. ^{207}Pb-NMR was used by Pecoraro and coworkers again with ZF peptides, this time to discern whether His imidazole ligands had any role in Pb(II) ligation. To confirm Pb-interacting species that they observed in the HIV-CCHC peptide, they

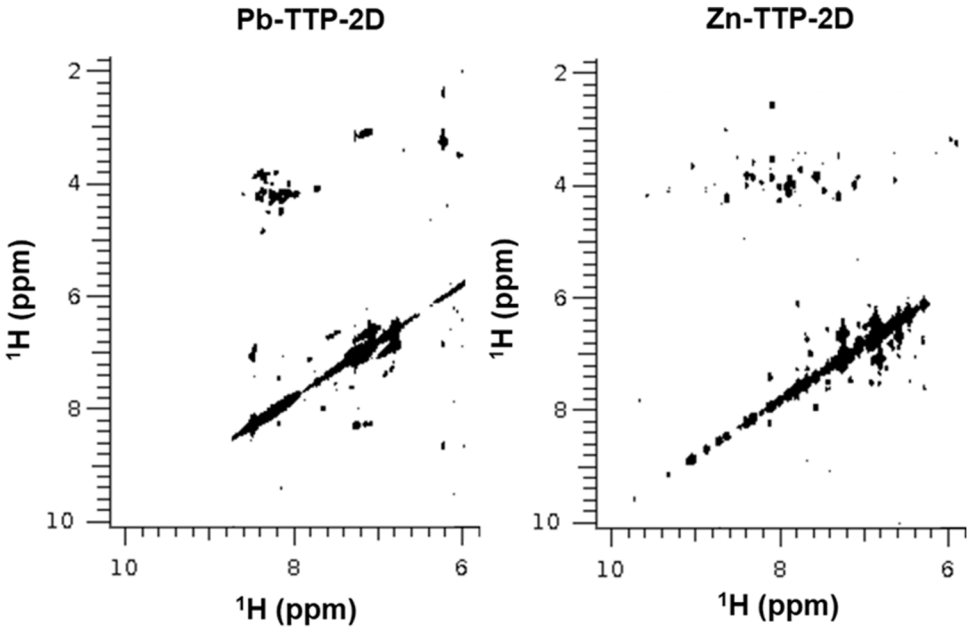

Fig. 4 Comparison of the 2-D ^{1}H-NMR COSY spectra from 6 to 10 ppm (x-axis) and 2 to 10 ppm (y-axis) Pb_2-TTP-2D (left) and Zn_2-TTP-2D (right) in 90% H_2O/10% D_2O. Samples were prepared at 350 µM peptide with 700 µM metal, adjusted to pH 6.5 with tris base

Table 2 Summary of EXAFS simulations data of Pb_2-TTP-2D

	Nearest-neighbor ligand environment[a]				Long-range ligand environment[a]				
Fit #	Atom[b]	*R* (Å)[c]	C.N.[d]	s^2 [e]	Atom[b]	*R* (Å)[c]	C.N.[d]	s^2 [e]	F'[f]
1	S	2.66	2.0	5.6	–	–	–	–	0.11
2	S	2.66	2.0	6.0	C	3.04	1.5	4.4	0.10
3	S	2.66	2.0	6.0	C	4.18	2.0	3.3	0.09

[a]Independent metal–ligand scattering environment

[b]Scattering atoms: S (sulfur) and C (carbon)

[c]Average metal–ligand bond length from two independent samples

[d]Average metal–ligand coordination number from two independent samples

[e]Average Debye–Waller factor in $Å^2 \times 10^3$ from two independent samples

[f]Number of degrees of freedom weighted mean square deviation between data and fit

also prepared and analyzed an HIV-CCGC peptide. The two peptides both exhibited similar spectra, ruling out the possibility of His participation [25]. In a related manner, Fig. S1 shows that in 1-D proton spectra of apo-TTP-2D, additions of Pb(II) did not chemically shift the non-exchangeable protons (~6 to 8 ppm region) of the His imidazole ring. This indicates that the His residues of TTP-2D (3 His in total) are not involved in coordinating Pb(II), as was found in Cd_2-TTP-2D [84], and supports the EXAFS fits that are optimized without N coordination. Taken together, the findings of PbS_3 coordination in Pb_2-TTP-2D (Fig. 5 and Table 2) are supported by previous studies of Pb(II) binding to sulfur-rich biomolecules.

Functional impact of Pb(II) mismetallation via TTP-2D/RNA interactions

The function of TTP to regulate cytokine mRNA is achieved via tight and specific binding of the ZF domains to ARE elements in the 3'UTR [98]. NMR analyses have revealed important hydrogen-bonding and pi-stacking interactions between the folded fingers of TTP and the adenosyl moieties of the ARE sequence, as well as the backbone of the RNA [41, 59, 99]. To determine the functional impact of Pb(II) binding of TTP-2D, a fluorescence anisotropy (FA) assay was employed to determine whether Pb_2-TTP-2D binds to a canonical ARE sequence. Our lab has previously reported that Zn_2-TTP-2D binds to the ARE sequence 5'-UUUAUU UAUUU-3' with nanomolar affinity [72]. This binding is selective, as Zn_2-TTP-2D exhibited 5- and 15-fold weaker affinity for two mutant oligonucleotides, 5'-UUU**G**UUU AUUU-3' and 5'-UUU**G**UUU**G**UUU-3'. Each of the RNAs were labeled with a 3' fluorescein tag to measure the RNAs anisotropy as a function of M-TTP-2D titrated into the cuvette.

We applied this FA assay to Pb_2-TTP-2D and report that, surprisingly, RNA-binding to the canonical ARE 11-mer is retained with Pb(II). Pb_2-TTP-2D binds the canonical ARE 11-mer with two orders of magnitude higher affinity than Zn_2-TTP-2D (760 pM versus 16 nM). Additionally, Pb_2-TTP-2D also binds to the oligonucleotides with a modified sequence much like Zn_2-TTP-2D does; however, the binding affinities of Pb_2-TTP-2D for these mutated sequences show a more significant decrease than that observed for Zn_2-TTP-2D. For example, the difference in binding affinity of Pb_2-TTP-2D for the canonical ARE sequence UUUAUUUAUUU versus the non-canonical ARE sequence UUU**G**UUU**G**UUU sequence is 100X, compared to 10X for Zn_2-TTP-2D with these same RNA sequences. Figure 6a plots the binding data and fits, and the dissociation constants (K_d) determined from the fits are summarized in Table 3. Figure 6b compares the K_ds for each metal and each RNA sequence. Collectively, these data show that despite the altered geometry and fold, Pb_2-TTP-2D exhibits tighter binding than Zn_2-TTP-2D to the 11-mer ARE. The RNA binding experiment for Pb_2-TTP-2D with the ARE mutants revealed that Pb_2-TTP-2D requires the adenosine nucleotides for tight binding and that Pb_2-TTP-2D's RNA binding is more specific than that of Zn_2-TTP-2D. Similar trends for RNA-binding were observed in Cd_2-TTP-2D, where Cd_2-TTP-2D bound the native 11-mer more tightly than Zn_2-TTP-2D but had greatly diminished binding with mutation of the RNA [84]. A key difference in this work is that Pb(II) adopts trigonal pyramidal geometry in TTP-2D, while Cd(II) likely maintains the native tetrahedral geometry.

Several groups have demonstrated diminished DNA- and RNA-binding of Pb-substituted ZFs, including Transcription Factor III A (TFIIIA), Specificity Protein-1 (Sp-1), and Early Growth Response (Egr-1) gene [49, 52, 53, 86, 100]. However, Zawia and coworkers proposed that the DNA binding of Sp-1 with Pb(II) may be biphasic, where it maintains function at low levels of Pb(II) but inhibits function with greater exposure. The Cys_4 GATA ZFs had markedly reduced DNA-binding activity both in vitro and in vivo (yeast), in gel-shift and LacZ-reporter assays, respectively [20]. In contrast, Hartwig and coworkers identified that Pb(II) did not affect the activity of two Cys_4 ZFs involved in DNA repair, Xeroderma Pigmentosum Complementation

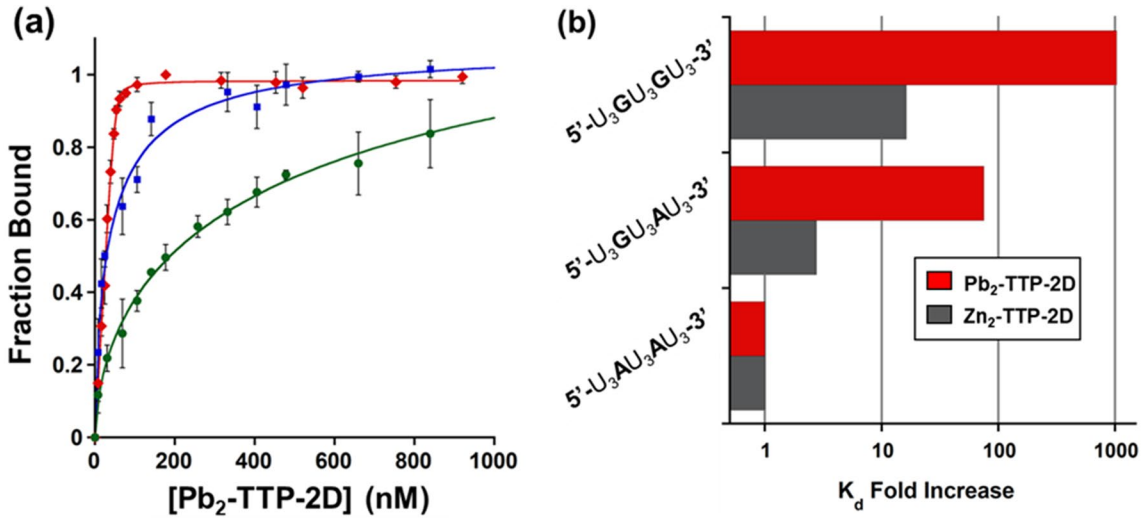

Fig. 6 **a** Plot of the change in anisotropy (as fraction bound) upon the addition of Pb_2-TTP-2D to the RNA oligonucleotides UUUAUUUAUUU-F (red), UUUGUUUAUUU-F (blue), and UUUGUUUGUUU-F (green). The solid lines represent a nonlinear least-squares fit to the binding model. **b** Comparison of M-TTP-2D affinity for ARE 11-mer oligonucleotides (fold increase = $K_{d\ Mutant}/K_{d\ Canonical}$) FA experiments were performed in 200 mM HEPES/100 mM NaCl/0.1 mg/mL BSA buffer at pH 7.5

Table 3 Dissociation constants (K_d) of M-TTP-2D [M = Pb(II), Zn(II)]

RNA sequences	Pb_2-TTP-2D	Zn_2-TTP-2 Da
UUU**A**UUU**A**UUU	0.760 ± 0.2 nM	16.0 ± 1.0 nM
UUU**G**UUU**A**UUU	57.0 ± 15 nM	44.0 ± 12 nM
UUU**G**UUU**G**UUU	780 ± 210 nM	260 ± 10 nM

[a]Reference [1]

Group A Protein (XPA) and bacterial formamidopyrimidine-DNA glycosylase (Fpg) [101]. The prokaryotic metal-sensing transcriptional regulators CadC and CmtR, both characterized by Giedroc and coworkers as containing PbS_3 coordination sites, are activated by Pb(II) binding [50, 102]. These two non-ZF examples are distinct, in that the apoprotein is inhibitory of DNA translation, but xenobiotic metal binding of the Cys_3 ligands is required for activation. Together, these data reveal that the effect of Pb binding to ZFs on oligonucleotide binding may be protein specific, with Pb inhibiting binding in some cases, enhancing binding in other cases, and having no effect in other cases.

Oxygen-rich side chains, as opposed to the Cys-rich sites discussed thus far, have been proposed as one of the ligating motifs for Pb(II) interaction with Ca(II)-binding proteins calmodulin (CaM) and troponin (TnC) [28, 30]. In the case of CaM, Yang and coworkers have demonstrated through several publications that Pb(II)'s interaction with CaM and the structure/function impact can occur in at least three ways; (1) Pb(II) can bind allosterically while Ca(II) is bound, or bind at the active metal site and either (2) inhibit or (3) hyperactivate CaM signaling [29, 31, 103]. Indeed, because TTP regulates itself (in addition to the other ZFP36 family members), hyperactivity with Pb_2-TTP could present a significant problem for cellular response to stress by diminishing TTP levels preemptively. Collectively, these data highlight that Pb(II)'s effect on metalloprotein function can be multifaceted and must be discerned by empirical studies for each specific protein.

Conclusions

Zinc finger proteins have been postulated for more than two decades as potential targets for the pathologic toxicity of Pb(II) and other toxic metals [11, 104]. This assertion is based upon the documented affinity of Pb(II), Cd(II), Hg(II), etc. for Cys-thiolate sites [12, 24, 25, 43, 96, 102]. The data presented here adds to a body of evidence for Pb(II) binding to biochemical sites, specifically those of Cys-rich metalloproteins. While Pb_2-TTP-2D does not exhibit the same secondary structure as exhibited by Zn_2-TTP-2D, it maintains tight binding to the canonical ARE RNA target sequence. Examples of both activating and inhibitory effects of Pb(II) substitution of ZFs have been described by others, and a pathogenic mechanism could be ascribed in either case. Indeed, as TTP also regulates its own expression by binding the 3'-UTR of TTP mRNA, hyperactivation of TTP activity, as seen in Pb(II) mismetallation of Ca(II)-binding proteins, could ultimately have a disruptive effect on TTP function by the depletion of TTP levels through auto-regulation. It is important to note that TTP requires PPIs of NOT1 and/

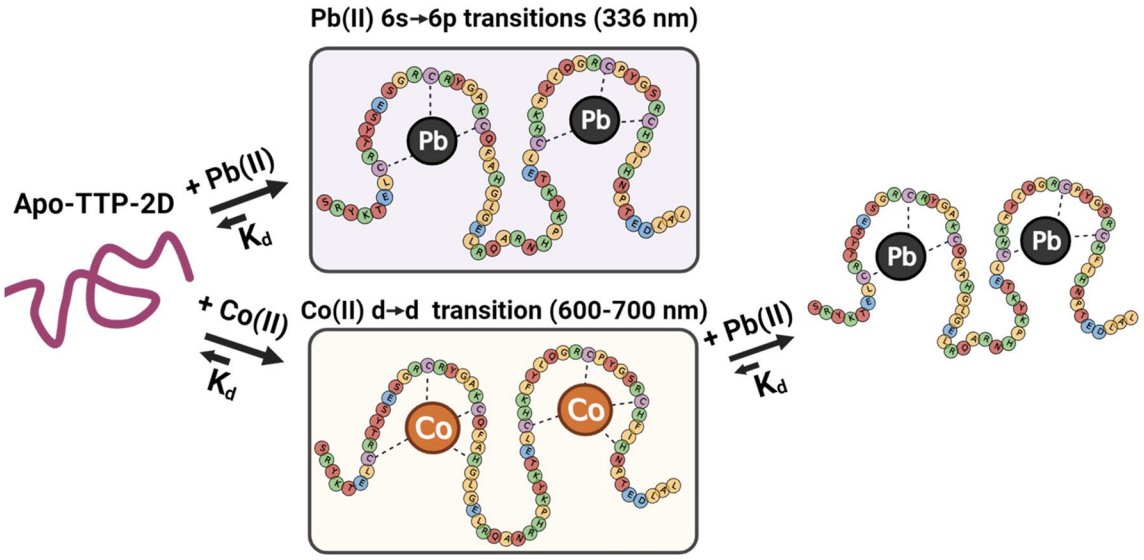

Scheme 2 Two different methods of UV–visible spectroscopy for determining Pb(II) metal binding affinity for apo-TTP-2D

or the decapping complex to destabilize target mRNAs [57, 58, 60], and that the altered fold of Pb_2-TTP-2D may not be suitable for these PPIs. Further work may consider the full picture of TTP activity and the effect that Pb(II) has on the many targets of TTP. Similarly, Pb(II) contributes to imbalance of inflammatory cytokines and the oxidative state of the cell, partly through its inhibition of glutathione reductase [17, 105]. Oxidation of zinc fingers, such as TTP, would perturb their intracellular levels and affect their ability to properly regulate cytokine levels. These broader implications of Pb(II) toxicity may provide ideas for future studies aimed at solving the multifaceted consequences of Pb(II) exposure with innovative therapies. Development of better prophylactic treatments and longitudinal screening of individuals exposed to Pb(II) are critical.

Supplementary Information The online version contains supplementary material available at https://doi.org/10.1007/s00775-022-01980-1.

Acknowledgements SLJM is grateful to the NSF (CHE-2106417). Synchrotron data was acquired at the Stanford Synchrotron Radiation Laboratory, which is supported by the NIH Research Resource Program and the US Department of Energy. The graphical abstract (includes PDB file 1RGO from Ref [55]) and Schemes 1 and 2 were created using Biorender with rights to publish.

Data availability All data generated and analyzed during this study are included in this published article (and the supplementary materials file).

Declarations

Conflict of interest The authors declare that they have no competing financial interests in any material discussed in this article.

References

1. Dignam T, Kaufmann RB, LeStourgeon L, Brown MJ (2019) Control of lead sources in the United States, 1970–2017: public health progress and current challenges to eliminating lead exposure. J Public Health Manag Pract 25(Suppl 1):S13–S22
2. Meyer PA, Brown MJ, Falk H (2008) Global approach to reducing lead exposure and poisoning. Mutat Res 659(1–2):166–175
3. Levin R, Brown MJ, Kashtock ME, Jacobs DE, Whelan EA, Rodman J, Schock MR, Padilla A, Sinks T (2008) Lead exposures in U.S. Children, 2008: implications for prevention. Environ Health Perspect 116:1285–1293
4. Pieper KJ, Tang M, Edwards MA (2017) Flint water crisis caused by interrupted corrosion control: investigating "ground zero" home. Environ Sci Technol 51:2007–2014
5. Pell MBSJ (2016) The thousands of US locales where lead poisoning is worse than in Flint. Reuters, London
6. Kennedy C, Yard E, Dignam T, Buchanan S, Condon S, Brown MJ, Raymond J, Rogers HS, Sarisky J, de Castro R, Arias I, Breysse P (2016) Blood lead levels among children aged < 6 years—Flint, Michigan, 2013–2016. MMWR Morb Mortal Wkly Rep 65:650–654
7. Rocha A, Trujillo KA (2019) Neurotoxicity of low-level lead exposure: history, mechanisms of action, and behavioral effects in humans and preclinical models. Neurotoxicology 73:58–80
8. Lanphear BP (1998) The paradox of lead poisoning prevention. Science 281:1617–1618
9. Dorea JG (2004) Mercury and lead during breast-feeding. Br J Nutr 92:21–40
10. Dorea JG, Donangelo CM (2006) Early (in uterus and infant) exposure to mercury and lead. Clin Nutr 25:369–376
11. Godwin HA (2001) The biological chemistry of lead. Curr Opin Chem Biol 5:223–227
12. Ordemann JM, Austin RN (2016) Lead neurotoxicity: exploring the potential impact of lead substitution in zinc-finger proteins on mental health. Metallomics 8:579–588
13. Hermes-Lima M, Pereira B, Bechara EJ (1991) Are free radicals involved in lead poisoning? Xenobiotica 21:1085–1090

14. Kasten-Jolly J, Pabello N, Bolivar VJ, Lawrence DA (2012) Developmental lead effects on behavior and brain gene expression in male and female BALB/cAnNTac mice. Neurotoxicology 33:1005–1020
15. Menon AV, Chang J, Kim J (2016) Mechanisms of divalent metal toxicity in affective disorders. Toxicology 339:58–72
16. Goering PL, Fowler BA (1987) Regulatory roles of high-affinity metal-binding proteins in mediating lead effects on d-aminolevulinic acid dehydratase. Ann N Y Acad Sci 514:235–247
17. Roels HA, Buchet JP, Lauwerys RR, Sonnet J (1975) Comparison of in vivo effect of inorganic lead and cadmium on glutathione reductase system and d-aminolevulinate dehydratase in human erythrocytes. Br J Ind Med 32:181–192
18. Pearson RG (2002) Hard and soft acids and bases. J Am Chem Soc 85:3533–3539
19. Kluska K, Adamczyk J, Krężel A (2018) Metal binding properties, stability and reactivity of zinc fingers. Coord Chem Rev 367:18–64
20. Ghering AB, Jenkins LM, Schenck BL, Deo S, Mayer RA, Pikaart MJ, Omichinski JG, Godwin HA (2005) Spectroscopic and functional determination of the interaction of Pb^{2+} with GATA proteins. J Am Chem Soc 127:3751–3759
21. Payne JC, ter Horst MA, Godwin HA (1999) Lead fingers: Pb^{2+} binding to structural zinc-binding domains determined directly by monitoring lead−thiolate charge-transfer bands. J Am Chem Soc 121:6850–6855
22. Cangelosi V, Ruckthong L, Pecoraro VL (2017) Lead(II) binding in natural and artificial proteins. Met Ions Life Sci 17:271–317
23. Magyar JS, Weng TC, Stern CM, Dye DF, Rous BW, Payne JC, Bridgewater BM, Mijovilovich A, Parkin G, Zaleski JM, Penner-Hahn JE, Godwin HA (2005) Reexamination of Lead(II) coordination preferences in sulfur-rich sites: implications for a critical mechanism of lead poisoning. J Am Chem Soc 127:9495–9505
24. Matzapetakis M, Ghosh D, Weng TC, Penner-Hahn JE, Pecoraro VL (2006) Peptidic models for the binding of Pb(II), Bi(III) and Cd(II) to mononuclear thiolate binding sites. J Biol Inorg Chem 11:876–890
25. Neupane KP, Pecoraro VL (2011) Pb-207 NMR spectroscopy reveals that Pb(II) coordinates with glutathione (GSH) and tris cysteine zinc finger proteins in a PbS3 coordination environment. J Inorg Biochem 105:1030–1034
26. Wong DL, Merrifield-MacRae ME, Stillman MJ (2017) Lead(II) binding in metallothioneins. Met Ions Life Sci 17:241
27. Zampella G, Neupane KP, De Gioia L, Pecoraro VL (2012) The importance of stereochemically active lone pairs for influencing Pb(II) and As(III) protein binding. Chemistry 18:2040–2050
28. Chao SH, Bu CH, Cheung WY (1990) Activation of troponin C by Cd^{2+} and Pb^{2+}. Arch Toxicol 64:490–496
29. Gorkhali R, Huang K, Kirberger M, Yang JJ (2016) Defining potential roles of Pb^{2+} in neurotoxicity rom a calciomics approach. Metallom Integr Biometal Sci 8:563–578
30. Habermann E, Crowell K, Janicki P (1983) Lead and other metals can substitute for Ca^{2+} in calmodulin. Arch Toxicol 54:61–70
31. Kirberger M, Wong HC, Jiang J, Yang JJ (2013) Metal toxicity and opportunistic binding of Pb^{2+} in proteins. J Inorg Biochem 125:40–49
32. Ok K, Filipovic MR, Michel SLJ (2021) Targeting zinc finger proteins with exogenous metals and molecules: lessons learned from tristetraprolin, a CCCH type zinc finger. Eur J Inorg Chem 2021:3795–3805
33. Pritts JD, Michel SLJ (2022) Fe-S clusters masquerading as zinc finger proteins. J Inorg Biochem 230:111756
34. Ok K, Li W, Neu HM, Batelu S, Stemmler TL, Kane MA, Michel SLJ (2020) Role of gold in inflammation and tristetraprolin activity. Chemistry 26:1535–1547
35. Bu S, Lv Y, Liu Y, Qiao S, Wang H (2021) Zinc finger proteins in neuro-related diseases progression. Front Neurosci 15:760567
36. Andreini C, Banci L, Bertini I, Rosato A (2006) Zinc through the three domains of life. J Proteome Res 5:3173–3178
37. Andreini C, Banci L, Bertini I, Rosato A (2006) Counting the zinc-proteins encoded in the human genome. J Proteome Res 5:196–201
38. Lee SJ, Michel SL (2014) Structural metal sites in nonclassical zinc finger proteins involved in transcriptional and translational regulation. Acc Chem Res 47:2643–2650
39. Michalek JL, Besold AN, Michel SL (2011) Cysteine and histidine shuffling: mixing and matching cysteine and histidine residues in zinc finger proteins to afford different folds and function. Dalton Trans 40:12619–12632
40. Cassandri M, Smirnov A, Novelli F, Pitolli C, Agostini M, Malewicz M, Melino G, Raschella G (2017) Zinc-finger proteins in health and disease. Cell Death Discov 3:17071
41. Amann BT, Worthington MT, Berg JM (2003) A Cys_3His zinc-binding domain from Nup475/Tristetraprolin: a novel fold with a disklike structure. Biochemistry 42:217–221
42. Gower-Winter SD, Levenson CW (2012) Zinc in the central nervous system: from molecules to behavior. BioFactors 38:186–193
43. Perez-Zuniga C, Leiva-Presa A, Austin RN, Capdevila M, Palacios O (2019) Pb(II) binding to the brain specific mammalian metallothionein isoform MT3 and its isolated αMT3 and βMT3 domains. Metallom Integr Biometal Sci 11:349–361
44. Habjanic J, Chesnov S, Zerbe O, Freisinger E (2020) Impact of naturally occurring serine/csteine variations on the structure and function of pseudomonas metallothioneins. Metallom Integr Biometal Sci 12:23–33
45. Ngu TT, Stillman MJ (2009) Metalation of metallothioneins. IUBMB Life 61:438–446
46. Blindauer CA (2011) Bacterial metallothioneins: past, present, and questions for the future. J Biol Inorg Chem 16:1011–1024
47. Cabral ACS, Jakovleska J, Deb A, Penner-Hahn JE, Pecoraro VL, Freisinger E (2018) Further insights into the metal ion binding abilities and the metalation pathway of a plant metallothionein from *Musa acuminata*. J Biol Inorg Chem 23:91–107
48. Belatik A, Hotchandani S, Carpentier R, Tajmir-Riahi HA (2012) Locating the BINDING SITes of Pb(II) ion with human and bovine serum albumins. PLoS ONE 7:e36723
49. Huang M, Krepkiy D, Hu W, Petering DH (2004) Zn-, Cd-, and Pb-transcription factor IIIA: properties, DNA binding, and comparison with TFIIIA-finger 3 metal complexes. J Inorg Biochem 98:775–785
50. Busenlehner LS, Cosper NJ, Scott RA, Rosen BP, Wong MD, Giedroc DP (2001) Spectroscopic properties of the metalloregulatory Cd(II) and Pb(II) sites of *S. aureus* pI258 CadC. Biochemistry 40:4426–4436
51. Basha MR, Wei W, Brydie M, Razmiafshari M, Zawia NH (2003) Lead-induced developmental perturbations in hippocampal Sp1 DNA-binding are prevented by zinc supplementation. in vivo evidence for Pb and Zn competition. Int J Dev Neurosci 21:1–12
52. Razmiafshari M, Zawia NH (2000) Utilization of a synthetic peptide as a tool to study the interaction of heavy metals with the zinc finger domain of proteins critical for gene expression in the developing brain. Toxicol Appl Pharmacol 166:1–12
53. Reddy GR, Zawia NH (2001) Lead exposure alters Egr-1 DNA-binding in the neonatal rat brain. Int J Dev Neurosci 18:791–795
54. Gao J, Chen YH, Peterson LC (2015) GATA family transcriptional factors: emerging suspects in hematologic disorders. Exp Hematol Oncol 4:28
55. Pikkarainen S, Tokola H, Kerkela R, Ruskoaho H (2004) GATA transcription factors in the developing and adult heart. Cardiovasc Res 63:196–207

56. Tiedje C, Diaz-Munoz MD, Trulley P, Ahlfors H, Laass K, Blackshear PJ, Turner M, Gaestel M (2016) The RNA-binding protein TTP is a global post-transcriptional regulator of feedback control in inflammation. Nucleic Acids Res 44:7418–7440
57. Maeda K, Akira S (2017) Regulation of mRNA stability by CCCH-type zinc-finger proteins in immune cells. Int Immunol 29:149–155
58. Yoshinaga M, Takeuchi O (2019) RNA binding proteins in the control of autoimmune diseases. Immunol Med 42:53–64
59. Hudson BP, Martinez-Yamout MA, Dyson HJ, Wright PE (2004) Recognition of the mRNA AU-rich element by the zinc finger domain of TIS11d. Nat Struct Mol Biol 11:257–264
60. Fu M, Blackshear PJ (2017) RNA-binding proteins in immune regulation: a focus on CCCH zinc finger proteins. Nat Rev Immunol 17:130–143
61. Alkallas R, Fish L, Goodarzi H, Najafabadi HS (2017) Inference of RNA decay rate from transcriptional profiling highlights the regulatory programs of Alzheimer's disease. Nat Commun 8:909
62. Guo J, Wang H, Jiang S, Xia J, Jin S (2017) The cross-talk between tristetraprolin and cytokines in cancer. Anticancer Agents Med Chem 17:1477–1486
63. Park JM, Lee TH, Kang TH (2018) Roles of tristetraprolin in tumorigenesis. Int J Mol Sci 19:3384
64. Tu Y, Wu X, Yu F, Dang J, Wang J, Wei Y, Cai Z, Zhou Z, Liao W, Li L, Zhang Y (2019) Tristetraprolin specifically regulates the expression and alternative splicing of immune response genes in HeLa cells. BMC Immunol 20:13
65. Sun X, Zhang H, Xie L, Qian C, Ye Y, Mao H, Wang B, Zhang H, Zhang Y, He X, Zhang S (2020) Tristetraprolin destabilizes NOX2 mRNA and protects dopaminergic neurons from oxidative damage in Parkinson's disease. FASEB J 34:15047–15061
66. Busada JT, Khadka S, Peterson KN, Druffner SR, Stumpo DJ, Zhou L, Oakley RH, Cidlowski JA, Blackshear PJ (2021) Tristetraprolin prevents gastric metaplasia in mice by suppressing pathogenic inflammation. Cell Mol Gastroenterol Hepatol 12:1831–1845
67. Rappl P, Brune B, Schmid T (2021) Role of tristetraprolin in the resolution of inflammation. Biology (Basel) 10:66
68. Taylor GA, Carballo E, Lee DM, Lai WS, Thompson MJ, Patel DD, Schenkman DI, Gilkeson GS, Broxmeyer HE, Haynes BF, Blackshear PJ (1996) A pathogenetic role for TNFα in the syndrome of cachexia, arthritis, and autoimmunity resulting from tristetraprolin (TTP) deficiency. Immunity 4:445–454
69. Neu HM, Lee A, Brandis JEP, Patel V, Schneider A, Kane MA, Dalby RN, Michel SLJ (2020) Cigalike electronic nicotine delivery systems e-liquids contain variable levels of metals. Sci Rep 10:11907
70. Cullen KA, Gentzke AS, Sawdey MD, Chang JT, Anic GM, Wang TW, Creamer MR, Jamal A, Ambrose BK, King BA (2019) E-Cigarette use among youth in the United States, 2019. JAMA 322:2095–2103
71. Dinardo P, Rome ES (2019) Vaping: the new wave of nicotine addiction. Cleve Clin J Med 86:789–798
72. diTargiani RC, Lee SJ, Wassink S, Michel SL (2006) Functional characterization of iron-substituted tristetraprolin-2D (TTP-2D, NUP475-2D): RNA binding affinity and selectivity. Biochemistry 45:13641–13649
73. Lee SJ, Michel SL (2010) Cysteine oxidation enhanced by iron in tristetraprolin, a zinc finger peptide. Inorg Chem 49:1211–1219
74. Besold AN, Lee SJ, Michel SL, Sue NL, Cymet HJ (2010) Functional characterization of iron-substituted neural zinc finger factor 1: metal and DNA binding. J Biol Inorg Chem 15:583–590
75. Doku RT, Park G, Wheeler KE, Splan KE (2013) Spectroscopic characterization of copper(I) binding to apo and metal-reconstituted zinc finger peptides. J Biol Inorg Chem 18:669–678
76. Chen X, Chu M, Giedroc DP (2000) Spectroscopic characterization of Co(II)-, Ni(II)-, and Cd(II)-substituted wild-type and non-native retroviral-type zinc finger peptides. J Biol Inorg Chem 5:93–101
77. Berg JM, Merkle DL (1989) On the metal ion specificity of zinc finger proteins. J Am Chem Soc 111:3759–3761
78. George GN, George SJ, Pickering IJ (2001) http://www-ssrl.slac.stanford.edu/~george/exafspak/exafs.htm, Menlo Park, CA
79. Rehr JJ, Ankudinov AL (2001) Progress and challenges in the theory and interpretation of X-ray spectra. J Synchrotron Radiat 8:61–65
80. Riggs-Gelasco PJ, Stemmler TL, Penner-Hahn JE (1995) XAFS of dinuclear metal sites in proteins and model compounds. Coord Chem Rev 114:245
81. Bencze KZ, Kondapalli KC, Stemmler TL (2007). In: Scott RA, Lukehart CM (eds) Applications of physical methods in inorganic and bioinorganic chemistry: handbook, encyclopedia of inorganic chemistry, 2nd edn. Wiley, Chichester, pp 513–528
82. Cotelesage JJ, Pushie MJ, Grochulski P, Pickering IJ, George GN (2012) Metalloprotein active site structure determination: synergy between X-ray absorption spectroscopy and X-ray crystallography. J Inorg Biochem 115:127–137
83. Al-Daghri NM, Al-Shuwaie AYA, Alghamdi A, Amer OE, Khattak MNK, Ansari MGA, Alnaami AM, Sabico S (2021) Tristetraprolin, inflammation, and metabolic syndrome in Arab adults: a case control study. Biology 10:550
84. Michalek JL, Lee SJ, Michel SL (2012) Cadmium coordination to the zinc binding domains of the non-classical zinc finger protein tristetraprolin affects RNA binding selectivity. J Inorg Biochem 112:32–38
85. Shimberg GD, Ok K, Neu HM, Splan KE, Michel SLJ (2017) Cu(I) disrupts the structure and function of the nonclassical zinc finger protein tristetraprolin (TTP). Inorg Chem 56:6838–6848
86. Sivo V, D'Abrosca G, Baglivo I, Iacovino R, Pedone PV, Fattorusso R, Russo L, Malgieri G, Isernia C (2019) Ni(II), Hg(II), and Pb(II) coordination in the prokaryotic zinc-finger Ros87. Inorg Chem 58:1067–1080
87. Pritts JD, Hursey MS, Michalek JL, Batelu S, Stemmler TL, Michel SLJ (2020) Unraveling the RNA binding properties of the iron-sulfur zinc finger protein CPSF30. Biochemistry 59:970–982
88. Busenlehner LS, Weng T-C, Penner-Hahn JE, Giedroc DP (2002) Elucidation of primary (α3N) and vestigial (α5) heavy metal-binding sites in *Staphylococcus aureus* pI258 CadC: evolutionary implications for metal ion selectivity of ArsR/SmtB metal sensor proteins. J Mol Biol 319:685–701
89. Mah V, Jalilehvand F (2012) Lead(II) complex formation with glutathione. Inorg Chem 51:6285–6298
90. Bertini ILC (1984) High spin Cobalt(II) as a probe for the investigation of metalloproteins. Adv Inorg Biochem 6:71–111
91. Imanishi M, Matsumura K, Tsuji S, Nakaya T, Negi S, Futaki S, Sugiura Y (2012) Zn(II) binding and DNA binding properties of ligand-substituted CXHH-type zinc finger proteins. Biochemistry 51:3342–3348
92. Krizek BA, Merkle DL, Berg JM (1993) Ligand variation and metal ion binding specificity in zinc finger peptides. Inorg Chem 32:937–940
93. Latt SA, Vallee BL (1971) Spectral properties of cobalt carboxypeptidase. the effects of substrates and inhibitors. Biochemistry 10:4263–4270
94. Brandis JEP, Zalesak SM, Kane MA, Michel SLJ (2021) Cadmium exchange with zinc in the non-classical zinc finger protein tristetraprolin. Inorg Chem 60:7697–7707
95. Sivo V, D'Abrosca G, Russo L, Iacovino R, Pedone PV, Fattorusso R, Isernia C, Malgieri G (2017) Co(II) coordination in

prokaryotic zinc finger domains as revealed by UV-Vis spectroscopy. Bioinorg Chem Appl 2017:1527247
96. Sisombath NS, Jalilehvand F (2015) Similarities between N-acetylcysteine and glutathione in binding to Lead(II) ions. Chem Res Toxicol 28:2313–2324
97. Schell AC, Parvez M, Jalilehvand F (2012) Redetermination of (d-penicillaminato)lead(II). Acta Crystallogr Sect E Struct Rep Online 68:m489-490
98. Blackshear PJ, Lai WS, Kennington EA, Brewer G, Wilson GM, Guan X, Zhou P (2003) Characteristics of the interaction of a synthetic human tristetraprolin tandem zinc finger peptide with AU-rich element-containing RNA substrates. J Biol Chem 278:19947–19955
99. Michel SL, Guerrerio AL, Berg JM (2003) Selective RNA binding by a Single CCCH Zinc-binding domain from Nup475 (tristetraprolin). Biochemistry 42:4626–4630
100. Hanas JS, Gunn CG (1996) Inhibition of transcription factor IIIA-DNA interactions by xenobiotic metal ions. Nucleic Acids Res 24:924–930
101. Asmuss M, Mullenders LH, Eker A, Hartwig A (2000) Differential effects of toxic metal compounds on the activities of Fpg and XPA, two zinc finger involved in DNA repair. Carcinogenesis 21:2097–2104
102. Wang Y, Hemmingsen L, Giedroc DP (2005) Structural and functional characterization of mycobacterium tuberculosis CmtR, a Pb^{II}/Cd^{II}-sensing SmtB/ArsR metalloregulatory repressor. Biochemistry 44:8976–8988
103. Kirberger M, Yang JJ (2008) Structural differences between Pb^{2+}- and Ca^{2+}-binding sites in proteins: implications with respect to toxicity. J Inorg Biochem 102:1901–1909
104. Hartwig A (2001) Zinc finger proteins as potential targets for toxic metal ions: differential effects on structure and function. Antioxid Redox Signal 3:625–634
105. Metryka E, Chibowska K, Gutowska I, Falkowska A, Kupnicka P, Barczak K, Chlubek D, Baranowska-Bosiacka I (2018) Lead (Pb) exposure enhances expression of factors associated with inflammation. Int J Mol Sci 19:1813

Authors and Affiliations

Andrew T. Stoltzfus[1] · Courtney J. Campbell[2] · Madison M. Worth[1] · Kellie Hom[1] · Timothy L. Stemmler[2] · Sarah L. J. Michel[1]

✉ Sarah L. J. Michel
smichel@rx.umaryland.edu

[1] Department of Pharmaceutical Sciences, University of Maryland School of Pharmacy, Baltimore, MD 21201, USA

[2] Department of Pharmaceutical Sciences, Wayne State University, Detroit, MI 48201, USA